Proceedings of the ASME 2013 International Mechanical Engineering Congress and Exposition
IMECE2013
November 15-21, 2013, San Diego, California, USA

IMECE2013-64281

2D PHASE-FIELD ANALYSES OF AXONAL EXTENSION OF NERVE CELL

K. NAKAGAWA
Graduate School of Doshisha University
Kyoto, Japan
dmm0024@mail4.doshisha.ac.jp

T. TAKAKI
Kyoto Institute of Technology
Kyoto, Japan
takaki@kit.ac.jp

Y. MORITA
Doshisha University
Kyoto, Japan
ymorita@mail.doshisha.ac.jp

E. NAKAMACHI
Doshisha University
Kyoto, Japan
enakamac@mail.doshisha.ac.jp

ABSTRACT

In this study, we aimed to develop a computer-aided simulation technique to predict the axonal extension in the neuronal network evolution processes for design new scaffolds to activate the nerve cell and promote the nerve regeneration. We developed a mathematical model of axonal extension by using phase-field method and evaluated the validity of the mathematical model by comparison with the experiments. In the previous experimental studies, the peripheral nerve scaffold has been introduced to guide the axonal extension. Damaged part of nerve was replaced by the artificial tube as the scaffold to induce the axonal growth through the artificial tube and regenerate the nerve network. However, the scaffold made of biodegradable materials has a problem that it is degraded and absorbed before the nerve regenerate, and then the nerve cannot regenerate. Therefore, there is a need for the design and development of a scaffold for nerve regeneration to promote nerve regeneration. For that purpose, it is necessary to understand the difference between the axonal extensions by the surrounding environment, such as the shape or materials of the scaffold for nerve regeneration. In particular, the numerical technique to analyze the remodeling process of the nerve in the scaffold is strongly required to be established because the in-vivo experimental observation technology at the micro scale, bioethical issues in the animal experiment and requires time and money are also remained as unresolved problems. In this study, we developed a new simulation code which employed the phase-field method to predict the two-dimensional dendritic and axonal growth processes of nerve cells on cultivation scaffolds. We curried out the phase-field analyses to make clear how the parameters of Kobayashi–Warren–Carter (KWC) phase-field model affected on the morphologic growths of dendrite and axon. Simultaneously, we had observed the axonal extension process by using the PC-12D cells with nerve growth factor (NGF) on two-dimensional cultivation dish. Based on these axonal extension observation results, we approximated the morphological changes and establish the phenomenological model for phase-field analysis. Finally, we confirmed the validity of our newly developed phase-field simulation scheme in two dimensions by comparison with the experiments.

INTRODUCTION

Reconstructive surgery has been performed on nerves damaged by traffic accidents, excision of malignancies, etc. employing the direct suture or autologous transplantation methods. However, the direct suture method is limited to cases where the length of the damaged nerve tube is 5 mm or less, and there often occurs the size mismatches between the donor and recipient tissue, the neuroma formation, and the loss of functionality at the donor sites. To overcome these problems, the re-generation therapy for the damaged nerve by using a scaffold has attracted attention [1-3].

The scaffold used for the nerve regeneration has the tube structure with sufficient strength to hold the lumen; it needs to be biodegradable and absorbable so that it does not damage the surrounding tissue and regenerated nerve [4-8]. The axonal extension should complete nerve regeneration before the scaffold biodegradation and absorption [9-12]. Therefore, an analysis scheme to predict the axonal extension process under consideration of scaffold effects is needed for design of the scaffold. However, because in vivo observation of experiments is difficult, a simulation technology to predict the axonal

extension is important to develop a scaffold for nerve regeneration. No effective numerical method has been developed so far because it is extremely difficult to predict the spontaneous extension and branching of an axon.

On the other hand, the phase-field method [13-18] has been applied in various fields of material science and engineering as a robust numerical scheme to solve the moving boundary phenomenon. In this study, we developed a new simulation code to predict the two-dimensional dendritic and axonal growth processes of nerve cells on cultivation scaffolds by using the phase-field method.

In a preliminary numerical study, we investigated the effects of two parameters of Kobayashi–Warren–Carter (KWC) model on the dendritic and axonal morphologic growths. Furthermore, we observed the axonal extension process of PC-12D cells in a two-dimensional cultivation medium to which nerve growth factor (NGF) was added. We compared the numerical results with the observation results of the axonal extension to confirm the validity of the newly developed phase-field simulation scheme.

CELL CULTURE AND TREATMENT

We performed a growth experiment on PC-12D cells to understand axonal extension process to develop a phase-field model. The PC-12D cells were cultured at 37°C under 5% CO2 in air with Dulbecco's modified Eagle's medium containing 10% horse serum and 10% fetal bovine serum. The cell density was adjusted to 2.5×10^4 cells/ml. We disseminated the cell suspension on a dish and added 50 ng/ml NGF to the dish after checking the adhesion of the cells. After adding NGF, we observed the cells in the incubator that was set on the microscope stage. Fig. 1 shows photomicrographs of the cell taken every 4 hrs. We found that four neurites were generated from a nerve cell body after certain periods from the beginning of observation; the axon grew from the neuritic tip. The nerve cell had a single axon; other neurites became dendrites. The axon extended into branches and came into contact with other dendrites extending from another nerve cell. When Sano [19] created an NGF gradient in the medium by using a micropipette, it was observed that the dendrites extended to the higher side of the concentration gradient.

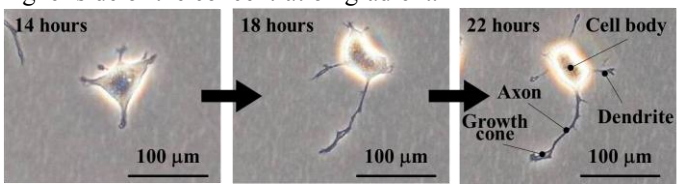

Fig. 1: Cultivated PC-12D cells every 4 hrs after exposure to NGF

PHASE FIELD MODEL

As shown in fig. 1, in the axonal growth experiment we first observed that several neurites sprouted from nerve cells after the providing NGF. We then observed that a thin axon grew from the neuritic tip and extended with branching.

This process of axonal extension was modeled using the phase-field method. To reproduce the branching in the growth cone, an orientation field and singular diffusion equations to express the orientation rotation are introduced. We adopted the KWC model [20-22], which was used to simulate the spherulite formation during solidification of the polymer material [23-25].

In this model, three order variables—the phase-field ϕ, orientation θ, and concentration c—are used. The phase-field ϕ takes a value of 1 in the cell and 0 in the solution (hereafter referred to as liquid); the solution surrounds the cell and includes nutritional factors such as NGF, ϕ changes smoothly at the interface region, as shown in fig. 2. The orientation θ was introduced to express axonal branching. The concentration c is the NGF concentration and expresses the fact that the axon grows by incorporating NGF. Following the Kim–Kim–Suzuki (KKS) model [26], the relationship of was assumed, where c_{cell} is the concentration inside the cell and c_{liq} is the concentration in the liquid. In addition, the ratio of c_{cell} and c_{liq} is set to be constant by the partition coefficient $k = c_{cell} / c_{liq}$.

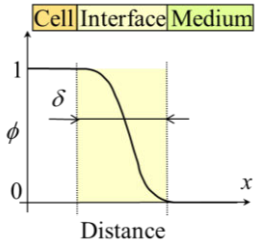

Fig. 2: Phase-field profile at interface region

The time evolution equations for ϕ, θ, and c are derived so that the total free energy of the system decreases monotonically with time. Here we use the following free energy function:

$$F = \int_V \left(f_{chem} + f_{doub} + f_{grad} + f_{orie} \right) dV \tag{1}$$

where f_{chem} is the free energy density of the bulk, f_{doub} is the double-well potential, f_{grad} is the gradient energy density and f_{orie} is the orientation gradient energy density. These are expressed as

$$f_{chem} = p(\phi) f^{cell} + (1 - p(\phi)) f^{liq} \tag{2}$$

$$f_{doub} = W q(\phi) \tag{3}$$

$$f_{grad} = \frac{a^2}{2} |\nabla \phi|^2 \tag{4}$$

$$f_{orie} = p(\phi) s |\nabla \theta| \tag{5}$$

where $p(\phi)$ is the monotonically increasing function denoted by $p(\phi) = \phi^3 (10 - 15\phi + 6\phi^2)$ and $q(\phi)$ is the double-well function denoted by $q(\phi) = \phi^2 (1 - \phi)^2$. a is the gradient coefficient considering the interface anisotropy. A normal function $a(\Theta) = \bar{a} \{1 + \xi \cos(\kappa(\Theta - \theta))\}$ is used, where Θ is the angle between the x-axis and interface normal, ξ is the anisotropy strength and κ is the anisotropy mode. The coefficients $\bar{a}$, W, s,

and M_ϕ can be related to the material parameters using the following equations:

$$\bar{a} = \sqrt{\frac{3\delta\gamma}{b}} \tag{6}$$

$$W = \frac{6\gamma b}{\delta} \tag{7}$$

$$s = \frac{a^2}{\delta} = \frac{3\gamma}{b} \tag{8}$$

$$M_\phi = \frac{\sqrt{2W}}{6a} M \tag{9}$$

where δ is the interface thickness, γ is the interface energy, and $b = 2\tanh^{-1}(1-2\lambda)$ is a constant related to the interface thickness, λ is the phase-field value for defining the interface region; $\lambda = 0.1$ was used here. f^{cell} is the energy density of the bulk inside the cell, and f^{liq} is the energy density of the bulk in the liquid. The following relationship was assumed for f^{cell} and f^{liq}:

$$\frac{\partial f^{cell}(c_{cell})}{\partial c_{cell}} = \frac{\partial f^{liq}(c_{liq})}{\partial c_{liq}} \tag{10}$$

The evolution equations of the phase-field ϕ, orientation θ, and concentration c are derived as

$$\frac{\partial\phi}{\partial t} = M_\phi \left[\begin{array}{l} \nabla(a^2\nabla\phi) - \frac{\partial}{\partial x}\left(a\frac{\partial a}{\partial\Theta}\frac{\partial\phi}{\partial y}\right) + \frac{\partial}{\partial y}\left(a\frac{\partial a}{\partial\Theta}\frac{\partial\phi}{\partial x}\right) \\ -\Delta f\frac{dp(\phi)}{d\phi} - W\frac{dq(\phi)}{d\phi} - 30q(\phi)s|\nabla\theta| \end{array} \right] \tag{11}$$

$$\frac{\partial\theta}{\partial t} = M_\theta \nabla\cdot\left[p(\phi)s\frac{\nabla\theta}{|\nabla\theta|} \right] \tag{12}$$

$$\frac{\partial c}{\partial t} = \nabla\cdot D\left[\nabla c + \frac{(1-k)c}{1-\phi+k\phi}\nabla\phi \right] \tag{13}$$

where M_ϕ is the phase-field mobility to determine the extension rate, M_θ is the orientation mobility to determine the frequency of axonal branching in the growth cone, and D is the diffusion coefficient of NGF. To maintain the thin axon morphology, the diffusion coefficient in the cell D_{cell} was set to be much larger than that in liquid D_{liq}. The diffusion coefficient is varied smoothly within the interface using the following equation:

$$D = D_{cell} + (D_{liq} - D_{cell})\frac{1-\phi}{1-\phi+k\phi} \tag{14}$$

In Eq. (11), Δf is the driving force and is expressed as

$$\Delta f = f^{liq}(c_{liq}) - f^{cell}(c_{cell}) - \frac{\partial f^{liq}(c_{liq})}{\partial c_{liq}}(c_{liq} - c_{cell}) \tag{15}$$

However, we used the following relation for simplicity:

$$\Delta f = S\Delta T \tag{16}$$

where S is the transformation entropy and ΔT is the change in temperature due to supercooling.

NUMERICAL SIMULATIONS

We carried out numerical simulations using the phase-field model derived in the previous section. First, we evaluated the effects of the initial orientation distribution, phase-field mobility and orientation mobility on the axonal extension morphology and determined the initial conditions and parameters. Finally, we performed axonal extension simulations and validated the model by comparing the results to results obtained from experimental observations.

Analysis conditions

Fig. 3 shows our analysis model and the initial conditions in the phase-field simulation and the blue region (ϕ = 1) indicates the cell morphology. The non-dimensional area of 1 × 1 was divided into the 1000 × 1000 finite difference grids. Thus, the grid size was $\Delta x = 0.001$. A circular cell body with a radius of $15\Delta x$ was placed in the center of the area. The initial concentrations were set to $c_{cell\_ini} = 0.5$ in the cell and $c_{liq\_ini} = 0.75$ in the liquid. The boundary condition was set to the zero Neumann boundary condition at all boundaries. The following parameters were employed: $\delta = 6\Delta x$, $\gamma = 1$, $D_{cell} = 10$, $D_{liq} = 1$, $k = 0.5$, $\kappa = 2$, $\xi = 0.5$, $M = 10$, $\Delta t = 4.0 \times 10^{-3}$. These parameters were assumed to express the nerve cell morphology.

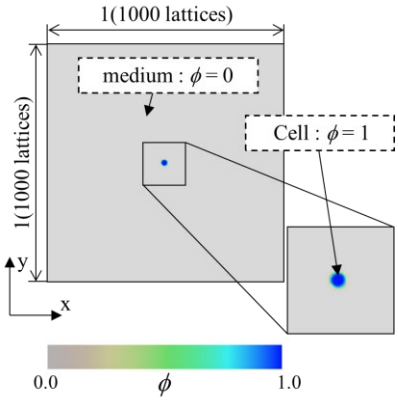

Fig. 3: Simulation model and initial conditions for ϕ in axonal growth simulations

Effects of initial orientation θ

We studied the effects of the orientation distribution inside and outside the cell on the axonal morphologic growth. Fig. 4 shows the calculated morphologies at every 50,000 step using $M_\theta / M_\phi = 0.5$. The left, center and right row figures show distribution of the phase-field variable ϕ, the orientation variable θ and the concentration c.

Here we set three kinds of initial orientation distributions: fig. 4 (a) to (c). Fig. 4 (a) is the result of that the all-region orientation is set to a constant value of 0. Fig. 4 (b) is that of the orientation in the cell is set to 0, and in the medium to random. Fig. 4 (c) is that of all orientation is set to random.

As shown in fig. 4 (a), we can see the straight morphology. The axon grew while almost maintaining the orientation of the

cell. On the other hand, in fig. 4 (b) two neurites grow as same to the fig. 4 (a), but we can see the changing the direction of the extension. And in fig. 4 (c), the multiple neurites extend to different directions, and, in the growth process, we can see the changing direction and the branching. Fig. 4 (c) shows us with an initial random orientation in the cell indicates that the neurites extended in various directions. As shown in fig. 1, because the cultivated nerve cell extended its neurites in various directions, the actual nerve extension can be expressed by setting the initial orientation inside and outside the cell to a random orientation.

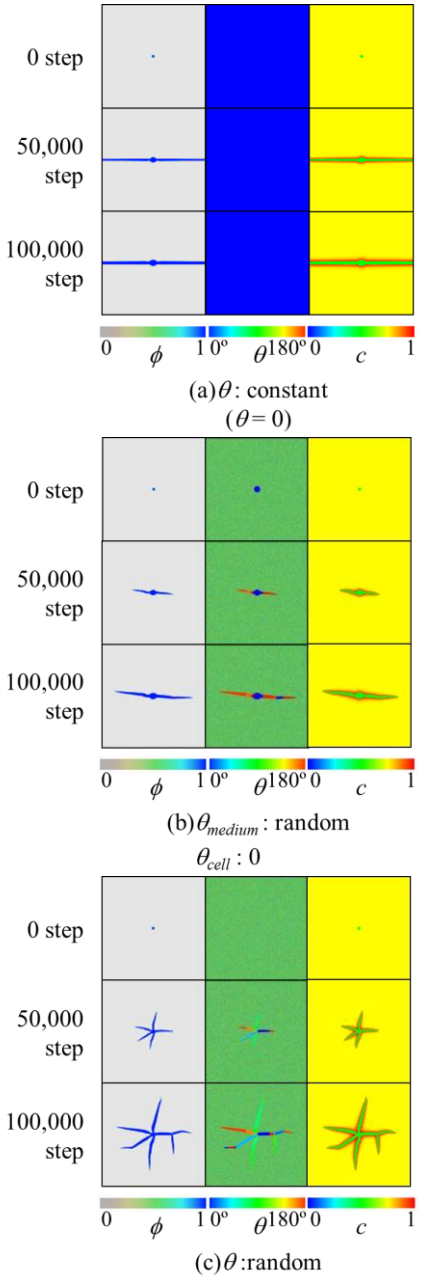

Fig. 4: Effects of initial orientation on axonal extension morphology

Effects of the phase-field mobility M_ϕ

We investigated the effects of the phase-field mobility M_ϕ on the morphology of axon in the phase-field simulation results. The phase-field simulations were carried out at M_ϕ = 0.3, 0.5, 0.7, and 1.0 under the condition of the all initial orientation was set to random. The calculated morphologies at every 50,000 step are shown in fig. 5 and the neurite lengths are measured in fig. 6.

From these results, we can understand the larger M_ϕ was set, the faster the extensions speed was. In addition, the larger M_ϕ was set, the higher the linearity of the axon was. So, by using the precise M_ϕ, we can fit the neurite extension speed and the linearity of the axon.

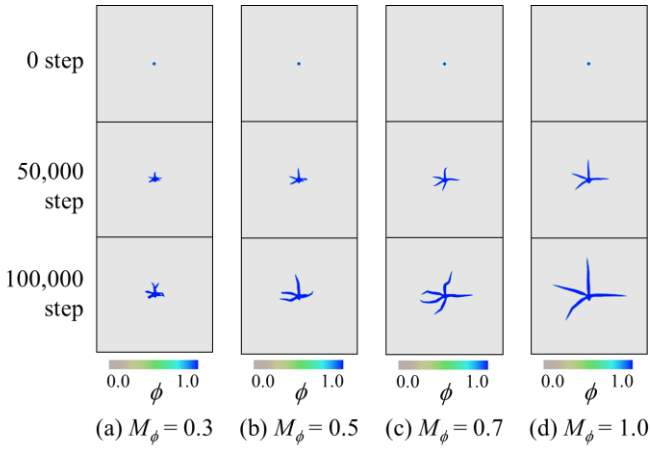

Fig. 5: Effects of phase-field mobility M_ϕ on axonal extension morphology

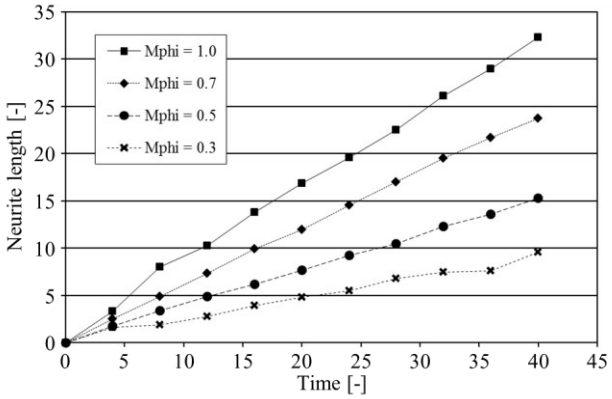

Fig. 6: Result of neurite length of M_ϕ = 0.3 to 1.0

Effects of the orientation mobility M_θ

We investigated the effects of the orientation mobility M_θ on the morphology of axon. The simulations were carried out at M_θ= 0.3, 0.5, 0.7, and 1.0 under the condition of the all initial orientation was set to random. The calculated morphologies at every 50,000 step are shown in fig. 7.

For small M_θ, the rotation speed of the orientation at the axonal tip was slow compared with the extension speed of the axonal tip. Therefore, the growth directions of the axonal tip tended to change because the orientation of the liquid was easily incorporated with the axonal tip. On the other hand, for large M_θ, the rotation speed of the orientation at the axonal tip was rapid compared with the extension speed of the axonal tip. Therefore, the growth direction remained constant because the orientation of the liquid was difficult to incorporate into the axon. From these results, we concluded that the axonal branch can be reproduced by selecting the orientation mobility M_θ.

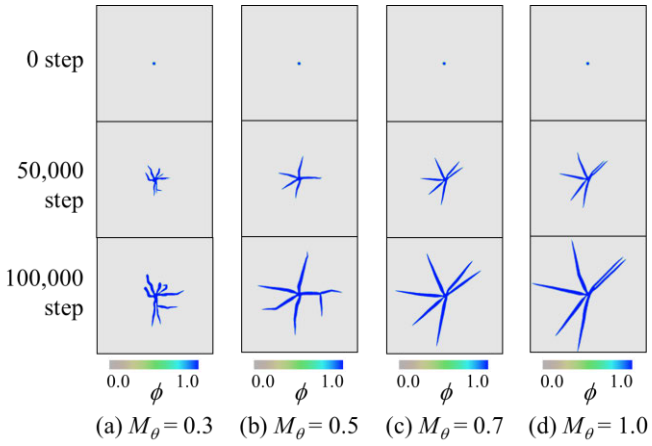

Fig. 7: Effects of orientation mobility M_θ on axonal extension morphology

Phase-field analyses of axonal extension of nerve cell

The preliminary computations presented in previous sections indicated that appropriate selection of orientation distribute, phase-field mobility M_ϕ and orientation mobility M_θ resulted in realistic axonal extension morphology. By considering these preliminary results, we simulated the axonal extension process. The validity of the developed model was confirmed by comparing its results to the results of the experimental observations. We employ random orientation at all region, $M_\phi = 1.0$ and $M_\theta = 0.5$.

Fig. 8 shows the results for the phase-field ϕ in the top row, orientation θ in the middle row, and concentration c in the bottom row at each step. Fig. 8 (a) shows the initial condition. We can see that all region orientation was set to random. As shown in fig. 8 (b), at 40,000 step, we found evidence that five neurites started to extend. In fig. 8 (c), at 80,000 step, which shows further cell growth at 40000 step, an axonal branch sprouted from one out of the five neurites. In fig. 8 (d), changes were observed in the dendritic growth direction, by incorporating the orientation of the liquid into the cell.

However, when comparing our results with the observation results, we could not express thin morphology of neuritis, the preferential extension of one neurite that resulted in the axon and growth cone at the tip of the axon.

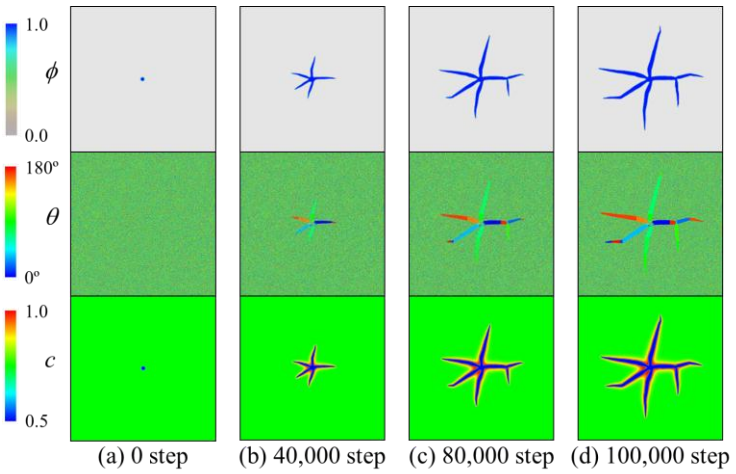

Fig. 8: Phase-field analyses of axonal extension of nerve cell

CONCLUSIONS

We developed a numerical model by applying the KWC phase-field model to predict the two-dimensional dendritic and axonal growth processes on the cultivation scaffolds.

We succeeded to predict the dendritic extension in various directions as observed for the initial growth of the nerve cell by setting the initial orientation inside the cell to a random orientation and selecting an appropriate M_ϕ and M_θ for the axonal branch.

When comparing our numerical results with our experimentally observation results, we could not predict accurately the facts that there occurs only one axon growth.

REFERENCES

[1] C. A. Heath and G. E. Rutkowski: The development of bioartificial nerve grafts for peripheral-nerve regeneration, *Trends Biotechnol*, Vol. 16 (1998), 163-168.

[2] G. R. D. Evans, et al.: Bioactive poly (L-lactic acid) conduits seeded with schwann cells for peripheral nerve regeneration, *Biomaterials*, Vol. 23 (2002), 841-848.

[3] I. V. Yannas, and B. J. Hill: Selection of biomaterials for peripheral nerve regeneration using data from the nerve chamber model, *Biomaterials*, Vol. 25 (2004), 1593-1600.

[4] T. Toba, et al.: Regeneration of canine peroneal nerve with the use of a polyglycolic acid–collagen tube filled with laminin-soaked collagen sponge: A comparative study of collagen sponge and collagen fibers as filling materials for nerve conduits, *J. Biomed. Mater. Res.*, Vol. 58 (2001), 622-630.

[5] T. Nakamura, et al.: Experimental study on the regeneration of peripheral nerve gaps through a polyglycolic acid–collagen (PGA–collagen) tube, *Brain Research*, Vol. 1027 (2004), 18-29.

[6] K. Matsumoto, et al.: Peripheral nerve regeneration across an 80-mm gap bridged by a polyglycolic acid

(PGA)–collagen tube filled with laminin-coated collagen fibers: a histological and electrophysiological evaluation of regenerated nerves, *Brain Research*, Vol. 868 (2000), 315-328.

[7] T. Kiyotani, et al.: Nerve regeneration across a 25-mm gap bridged by a polyglycolic acid-collagen tube: a histological and electrophysiological evaluation of regenerated nerves, *Brain Research*, Vol. 740 (1996), 66-74.

[8] A. Hagiwara, et al.: Clinical application of PGA-tube for regeneration intrapelvic nerves during extended surgery for intrapelvic recurrent rectal cancer, *Japanese Journal of Cancer and Chemotherapy*, Vol.29 (2002), 2202－2204.

[9] G. R. D. Evans, et al.: In vivo evaluation of poly (L-lactic acid) porous conduits for peripheral nerve regeneration, *Biomaterials*, Vol. 20 (1999), 109-1115.

[10] J. Li, and R. Shi: Fabrication of patterned multi-walled poly-l-lactic acid conduits for nerve regeneration, *Journal of Neuroscience Methods*, Vol. 165 (2007), 257-264.

[11] A. K. Kitahara, et al.: Evaluation of collagen nerve guide in facial nerve regeneration, *The Japanese Society for Artificial Organs*, Vol. 1 (1998), 22-27.

[12] F. Langone, et al.: Peripheral nerve repair using a poly(organo)phosphazene tubular prosthesis, *Biomaterials*, Vol. 16 (1995), 347-353.

[13] J. A. Warren, et al.: Extending phase field models of solidification to polycrystalline materials, *Acta Materialia*, Vol. 51 (2003), 6035-6058.

[14] R. Kobayashi: Modeling and numerical simulations of dendritic crystal growth, *physica D*, Vol.63 (1993), 410-423.

[15] A. Karma, et al.: Quantitative phase-field modeling of dendritic growth in two and three dimensions, *Phys. Rev. E*, Vol. 57 (1998), 4323-4349.

[16] M. Ode, et al.: Phase-field model for solidification of ternary alloys, *ISIJ Int.*, Vol. 40 (2000), 870-876.

[17] Y. Natsume, et al.: Phase-field Simulation of Transient Liquid Phase Bonding Process of Ni Using Ni－P Binary Filler Metal, *Mater. Trans.*, Vol. 44 (2003), 819-823.

[18] Y. Natsume, et al.: Analysis of Growth Behavior of a Cellular and Dendritic Interface under a Constrained Growth Condition using a Phase-Field Model, *Mater. Trans.*, Vol.44 (2003), 824-828.

[19] M. Sano: A new model for the study of the cellular action of NGF, PC12D cell, *J. Kyoto Pref. Univ. Med*, Vol. 108 (1999), 667-678.

[20] R. Kobayashi, J. A. Warren, and W. C. Carter: Vector-valued phase field model for crystallizetion and grain boundary formation. *Physica D*, Vol. 119 (1998), 415-423.

[21] R. Kobayashi, J. A. Warren, and W. C. Carter: A continuum model of grain boundaries, *Physica D*, Vol.140 (2000), 141-150.

[22] J. A. Warren, R. Kobayashi, and W. C. Carter: Modeling grain boundaries using a phase-field technique, *J. Cryst. Growth*, vol.211 (2000), 18-20.

[23] L. Gránásy, T. Pusztai, T. Börzsönyi, J. A. Warren, and J. F. Douglas: A general mechanism of polycrystalline growth. *Nature materials*, Vol. 3 (2004), 645-650.

[24] L. Gránásy, T. Pusztai, and J. A. Warren: Modeling polycrystalline solidification using phase field theory. *Journal of Physics: Condensed Matter*, Vol. 16 (2004), R1205-R1235.

[25] M. Asanishi, T. Takaki, and Y. Tomita: Polymer spherulite growth simulation during crystallization by phase-field method, *Proceedings of International Conference on Advances and Trends in Engineering Materials and Their Applications*, (2007), 195-203.

[26] S. G. Kim, et al.： Phase-field model for binary alloys, *Phys. Rev. E*, Vol. 60 (1999), 7186-7197.